

PLATE I

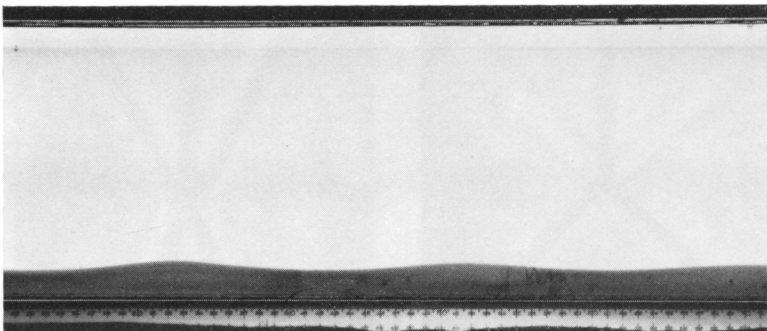


Fig. 2.1. A wave on the interface between two homogeneous fluid layers with different densities and depths. The lower layer is dyed.

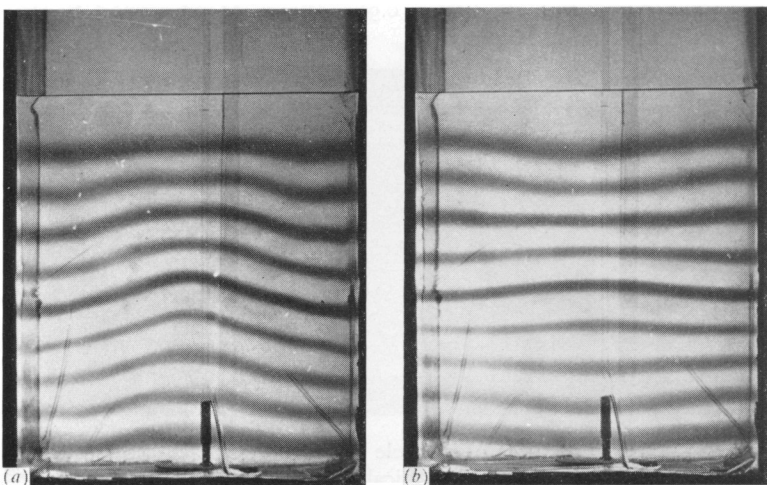


Fig. 2.6. Laboratory experiments on standing internal waves in a continuously stratified fluid (a) mode (2, 1), (b) mode (2, 3). The dyed layers marking surfaces of constant density were inserted during the filling of the tank. (From Thorpe 1968a.)

PLATE II

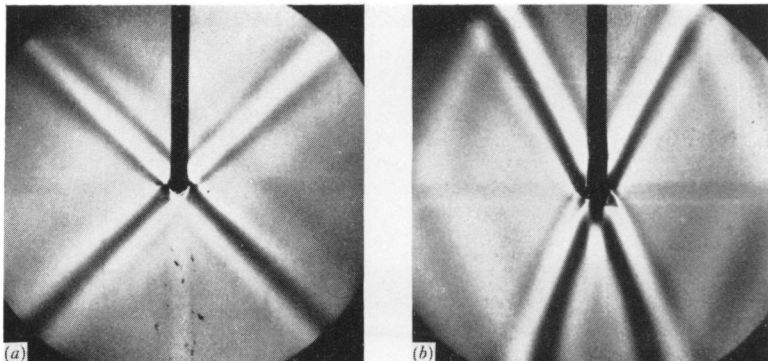


Fig. 2.7. Schlieren pictures of the density variations produced by internal waves propagating along rays and originating at a horizontally oscillated body (a) $\omega/N = 0.615$, (b) $\omega/N = 0.900$. (From Mowbray and Rarity 1967.)

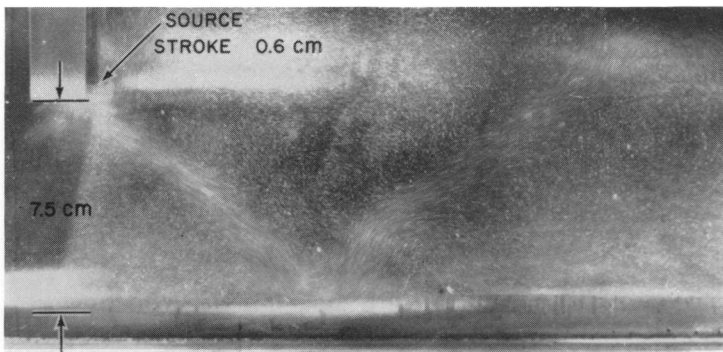


Fig. 2.11. Streak pictures of particle motions associated with internal waves propagating away from a vertically oscillated source ($\omega/N = 0.60$).

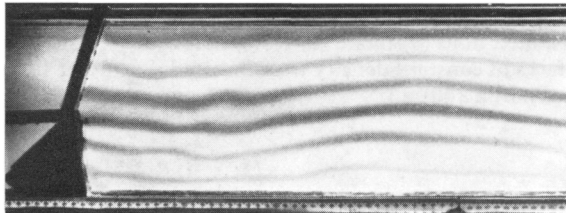


Fig. 2.12. Waves produced by oscillating a flap at one end of a tank of salt solution with linear density gradient. Disturbances described by the 'mode' and 'ray' theories can both be seen. (From Thorpe 1968c.)

PLATE III

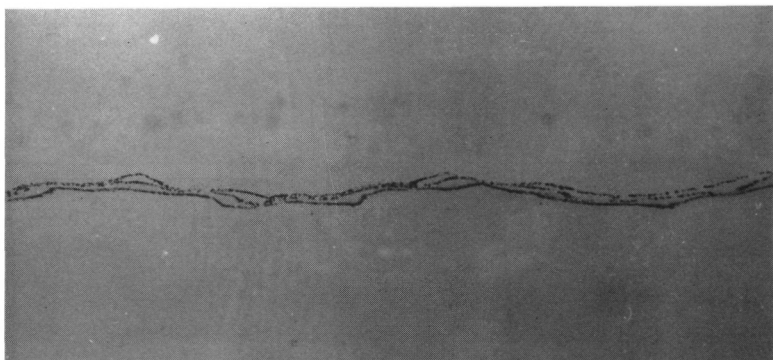
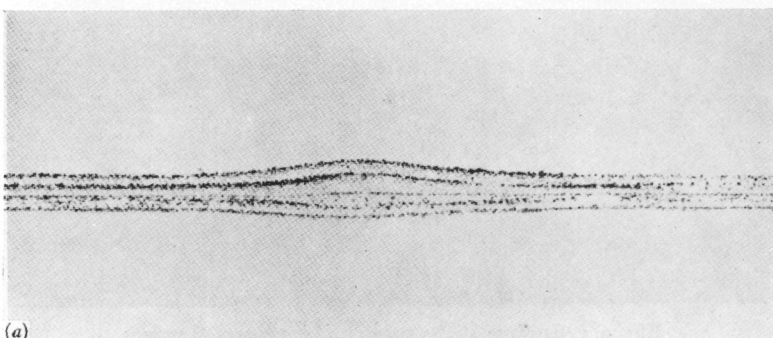


Fig. 2.18. Instability of an interfacial wave caused by the growth of higher modes by resonant interaction. (From Davis and Acrivos 1967*b*.)



(a)

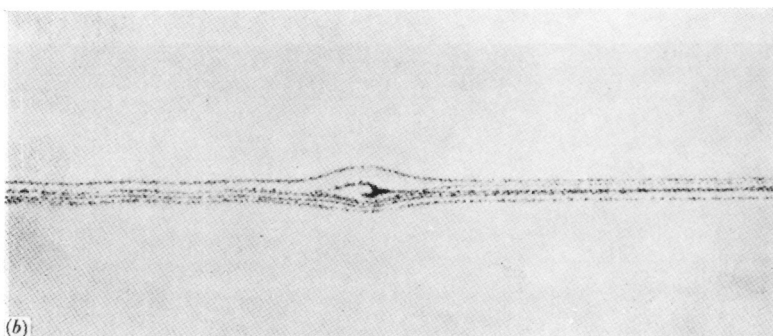


Fig. 3.3. Solitary waves on an interfacial transition region between two layers (a) small amplitude, (b) large amplitude, showing closed streamlines. (From Davis and Acrivos 1967*a*.)

PLATE IV



Fig. 2.3. Surface slicks produced by internal waves
(British Columbia Air Photographic Service).

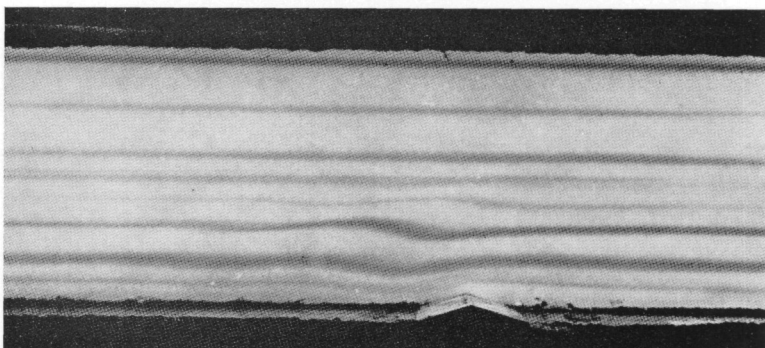


Fig. 2.15. Absorption of energy at a critical level in a shear flow: lee waves cannot penetrate beyond the centre-line of the channel where $u = 0$.
(From Hazel 1967.)

PLATE V

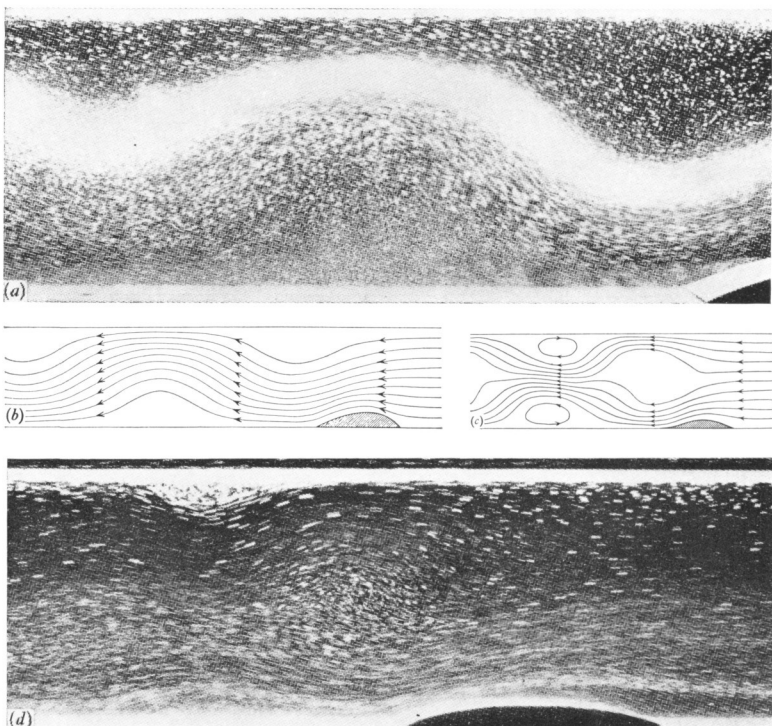


Fig. 3.4. Stratified flow (from right to left) over a barrier in a channel. (a), (b) Comparison between observed/calculated flow patterns, with one lee mode present and parameters (defined following (3.1.18)) $\kappa = 0.60/0.65$ and $\epsilon = 0.27/0.38$. (From Long 1955.) (d), (c) Comparison between observed/calculated flow patterns for a case where there are two lee modes, and rotors are formed; $\kappa = 0.65/0.70$, $\epsilon = 0.17/0.15$. (From Long 1955.)

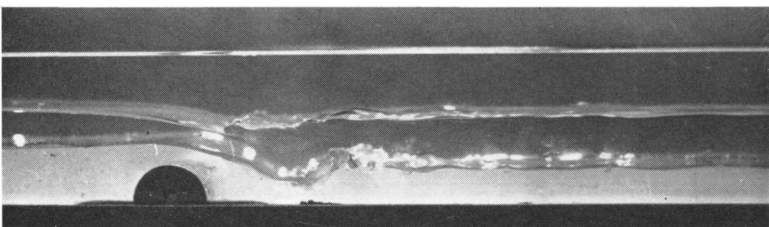


Fig. 3.10. Flow of a three-layer fluid system over a ridge, produced by moving a two-dimensional obstacle from right to left. There is a weak hydraulic jump on the upper interface near the obstacle, and a stronger jump downstream on the lower interface; the latter can be compared to the Sierra Wave phenomenon shown in fig. 3.11 pl. vi. (From Long 1953b.)

PLATE VI



Fig. 3.11. A hydraulic jump in a supercritical airflow over the Sierra Nevada range, made visible by the formation of cloud, and by dust raised from the ground in the turbulent flow behind the jump. (Photograph by Robert Symons, published in *Communications on Pure and Applied Maths*, 20, no. 2 (review by M. J. Lighthill), © John Wiley & Sons, Inc., 1967.)



Fig. 3.14. The front of a gravity current in the atmosphere: a Sudanese haboob, in which thick dust swept up by a cold outflow from a thunder-storm contributes to the density difference which drives the flow. Note the overhang, and the clefts in the front which are probably associated with convective motions arising from the unstable density distribution near the ground. (Photograph: Flight International.)

PLATE VII

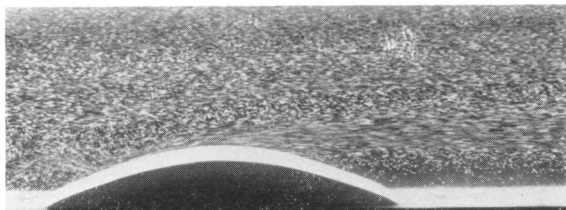


Fig. 3.18. Streak picture of a very slow flow (from right to left) over a high barrier, showing the complete blocking upstream of the obstacle, and the formation of multiple jets. (From Long 1955.)

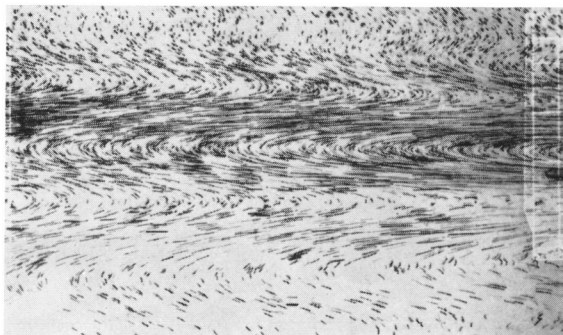


Fig. 3.21. Streak picture of an upstream wake, produced by a plate moving from right to left; camera stationary, centred about 10 cm upstream. (From Pao (1968), Boeing Scientific Labs. Document D1-82-0488.)

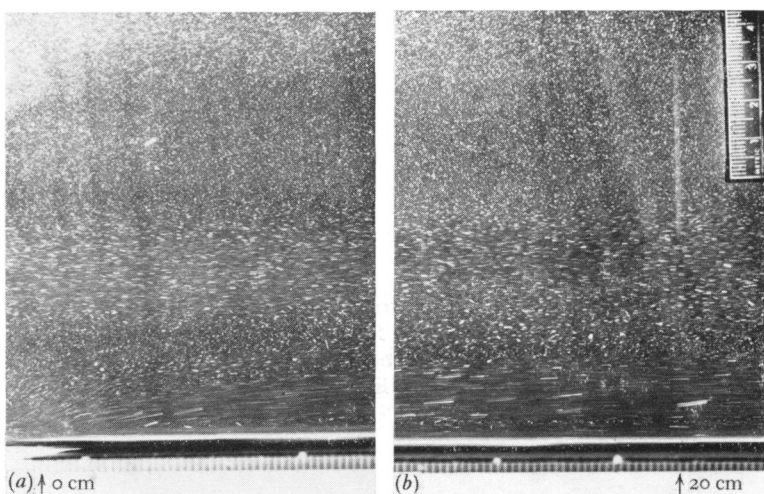


Fig. 3.22. The upstream boundary layer, at two positions along a plate moving from left to right past a stationary camera. The alternating jet structure, and the growth of the boundary layer with distance from the back of the plate, are clearly shown. (From Martin 1966.)

PLATE VIII

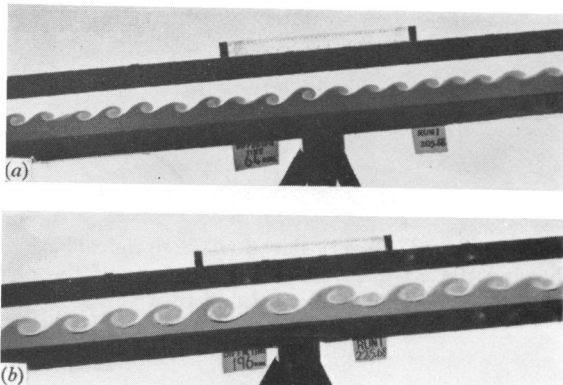


Fig. 4.10. The breakdown of a density interface in a shear flow produced by tilting the containing tube. The interface in (b) has been allowed to diffuse (and thicken) about three times as long as that in (a). (From Thorpe 1971.)

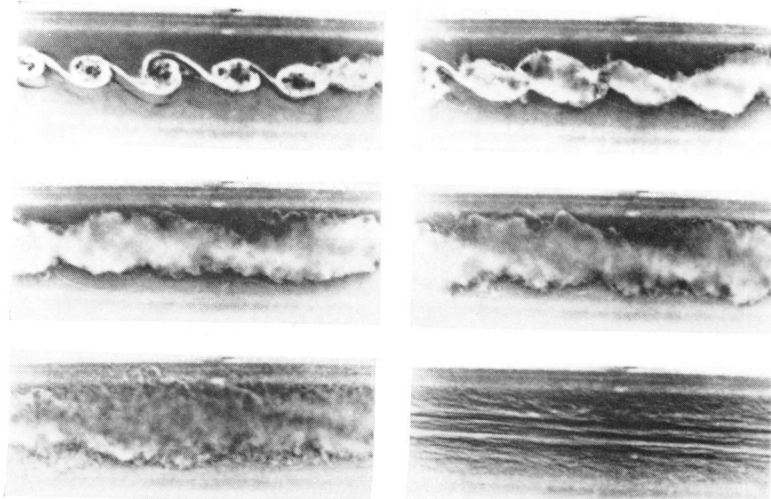


Fig. 4.12. A sequence of shadowgraph pictures of a density interface subjected to a steady shear. Reading from left to right, top to bottom, an instability of the K-H form grows, turbulence is produced, the interface thickens and finally the turbulence is suppressed. (From Thorpe 1971.)

PLATE IX

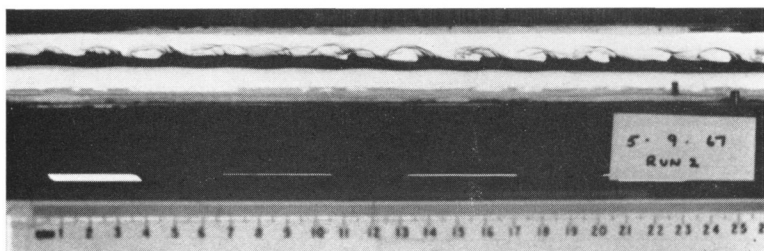


Fig. 4.13. 'Cusped' breaking waves on the interface between the layers which follow two noses advancing in opposite directions along a closed tube (the lock exchange flow). (From Thorpe 1968*b*.)

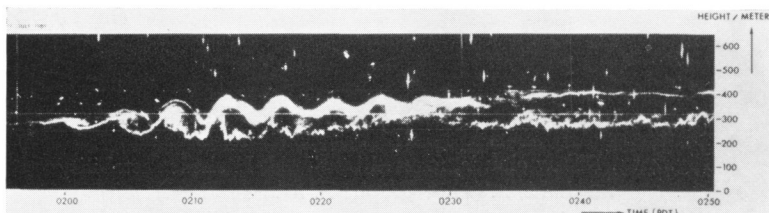


Fig. 4.15. Time-height record of growing and overturning waves obtained using radar in clear air. (From Atlas *et al.* 1970.)

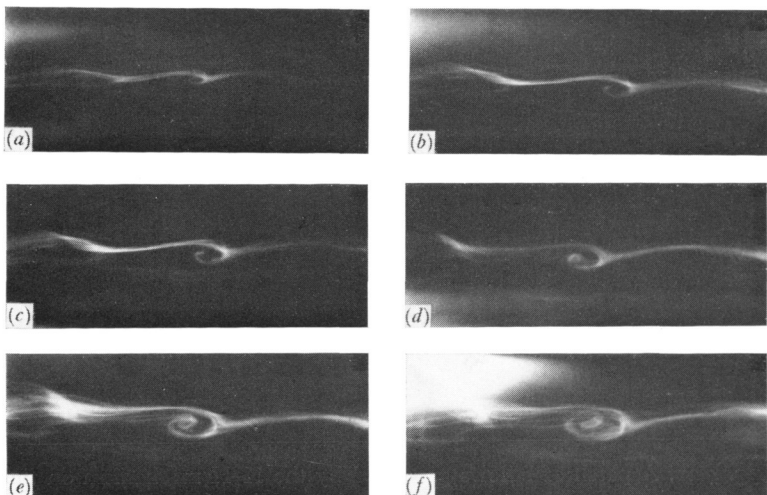


Fig. 4.20. Stages in the development of a billow produced by a long wave travelling along an interface in the thermocline. (From Woods 1968*b*.)

PLATE X



Fig. 4.14. Billow clouds, formed by the K-H shear instability mechanism. (Photograph: P. M. Saunders.)

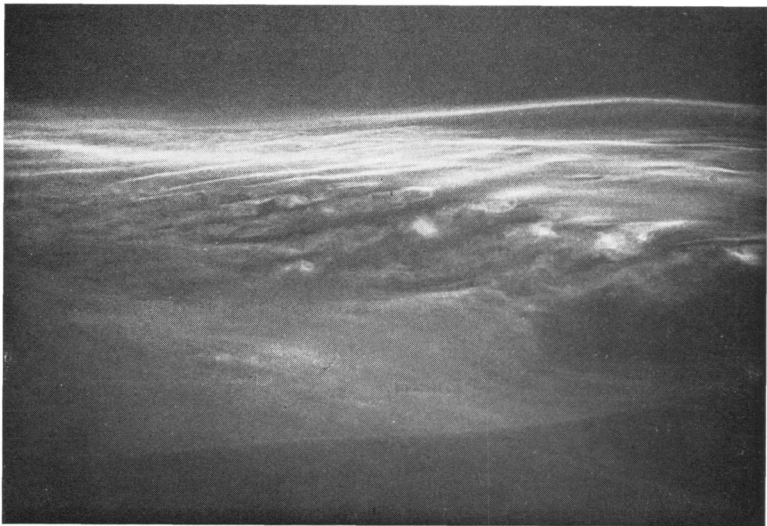


Fig. 4.21. A patch of billows produced by the K-H mechanism on the crest of a 10 m long internal wave on a thermocline sheet. (From Woods 1968*b*.)

PLATE XI



Fig. 4.23. Clouds formed by lee waves over a mountain. The lowest cloud is associated with a turbulent rotor; above it is a smooth lenticular cloud formed on a wave crest which is not overturning. (Photograph: Betsy Woodward.)



Fig. 7.2. Convective clouds in an unstable layer, aligned in 'streets' along the direction of shear. (Compare with fig. 4.14 pl. x, which shows clouds formed by a shear instability and aligned across the flow. The form of 'billow' clouds can vary widely according to the relative importance of shear and convection.) (Photograph: R. S. Scorer.)

PLATE XII

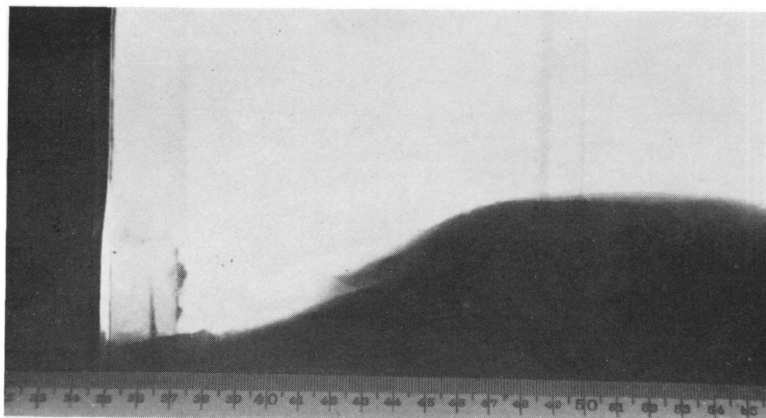


Fig. 4.22. Shear instability occurring at a node of a standing interfacial gravity wave. (From Thorpe 1968*a*.)

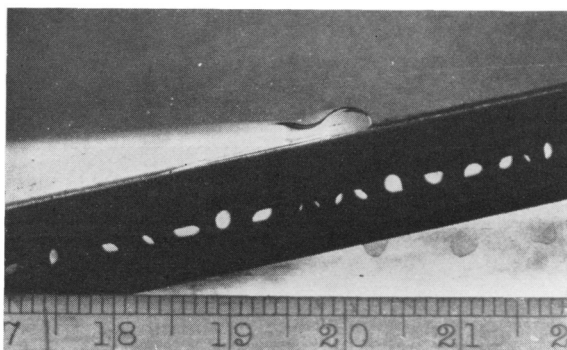


Fig. 4.24. The breaking of an interfacial wave as it approaches a slope. (From Thorpe 1966*a*.)

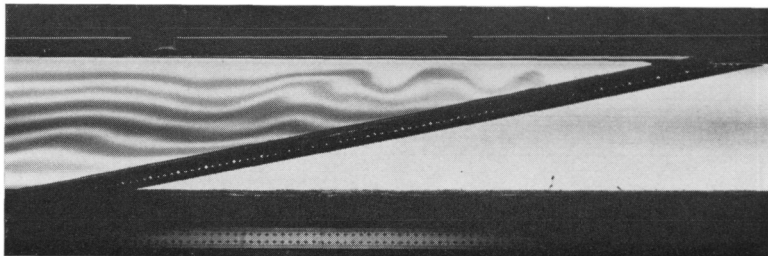


Fig. 4.25. The breaking of an internal wave in a continuous density gradient as it approaches a slope. (From Thorpe 1966*a*.)

PLATE XIII

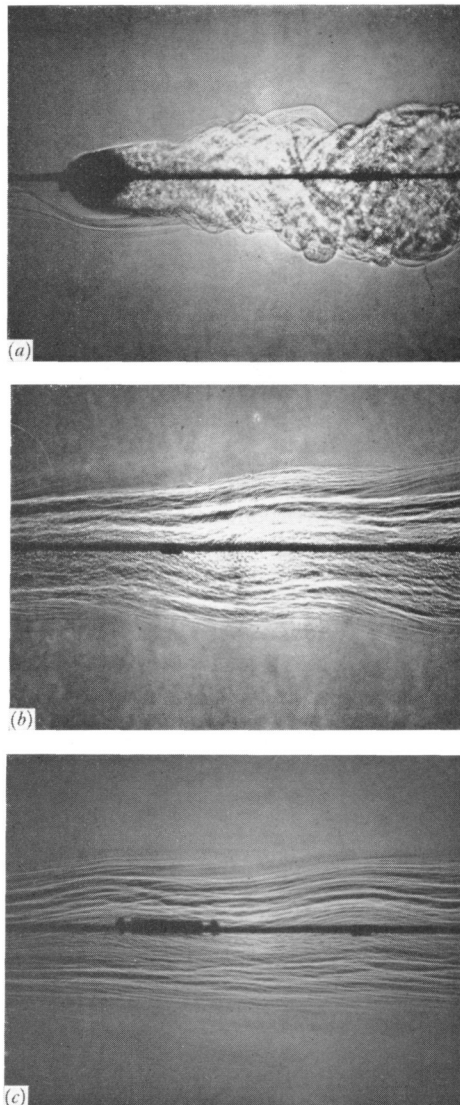


Fig. 5.10. Shadowgraph pictures due to Pao (1968*b*), of a turbulent wake behind a circular cylinder in a stratified fluid (*a*) near the body: the wake resembles that in a homogeneous fluid, (*b*) 50 diameters behind the body: the large scale motions have been damped, (*c*) 100 diameters behind the body: the fine structure has also decayed, leaving horizontal striations of concentration. (From Pao (1968), Boeing Scientific Labs. Document D1-82-0959.)

PLATE XIV

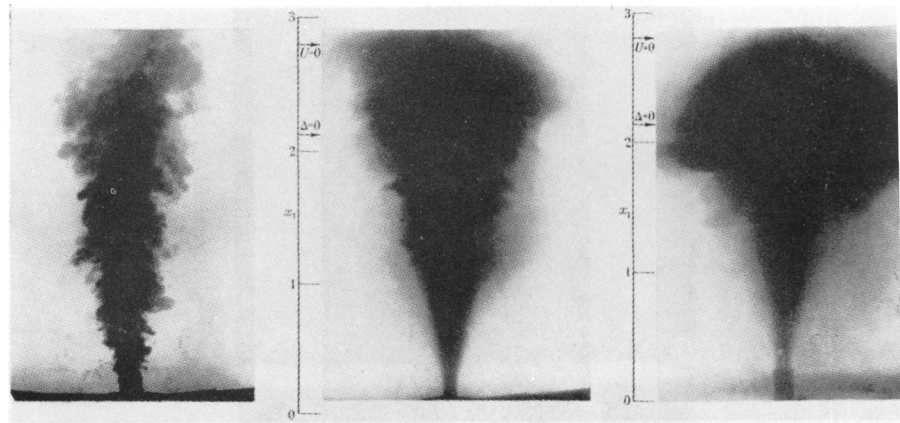


Fig. 6.2. Steady turbulent plumes of dyed buoyant fluid (a) in a uniform environment, with a short exposure which shows the large eddy structure, (b) in a stably stratified environment: a time exposure during an early stage of release, (c) in a stably stratified fluid: a time exposure at a later stage when a layer is spreading out sideways at the top. (From Morton, Taylor and Turner 1956.)

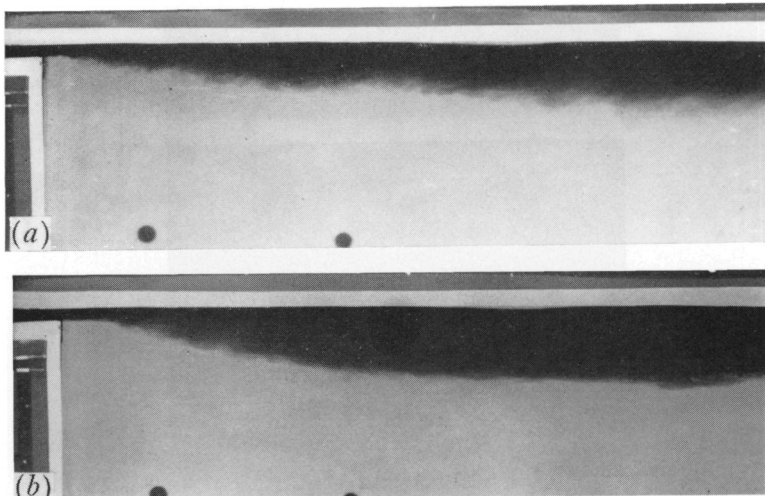


Fig. 6.9. (a) An internal hydraulic jump of the maximum entraining type, with entrainment along its whole length. (b) An internal hydraulic jump controlled by a broad-crested weir downstream: the flow upstream of the jump is identical to that in (a). Entrainment is occurring only at the far upstream end of the jump, and the remainder consists of a roller zone. (From Wilkinson and Wood 1971.)

PLATE XV

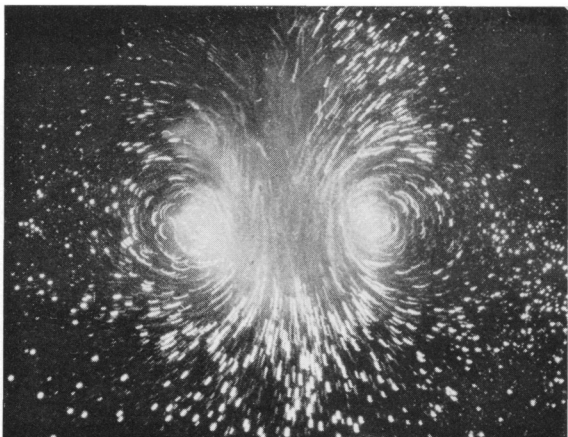


Fig. 6.13. Streak picture of the flow in and around an isolated thermal of dyed salt solution, showing approximate streamlines relative to axes at rest. (Photograph by P. M. Saunders.)

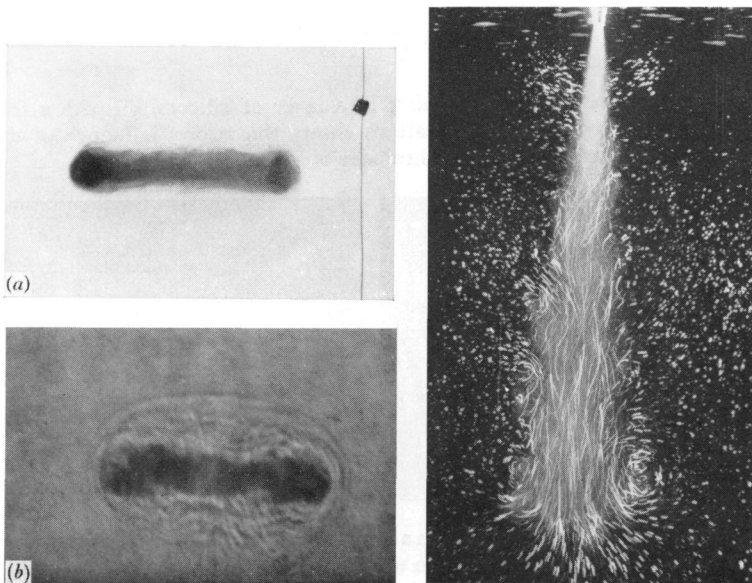


Fig. 6.15. (Left.) Buoyant vortex rings. (a) A turbulent, buoyant core. (b) A shadowgraph picture, showing the buoyant core and the surrounding volume of fluid which is carried along with it.

Fig. 6.16. (Right.) Streak picture of a 'starting plume' of salt solution in fresh water, showing the cap (resembling a thermal) followed by a steady turbulent plume.

PLATE XVI

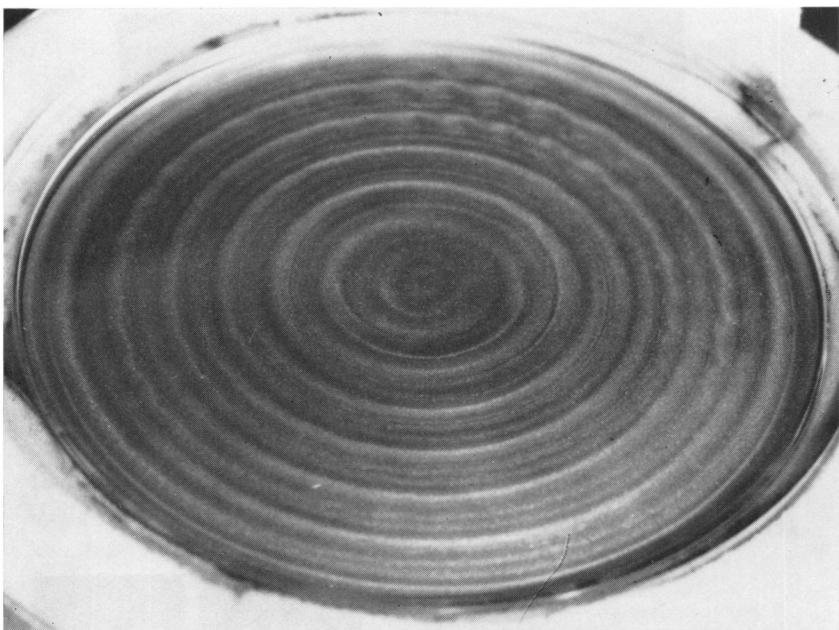


Fig. 7.3. Convection rolls forming in a layer of silicone oil with a free surface. The concentric ring pattern shows the strong influence of the circular boundary. (From Koschmieder 1967.)

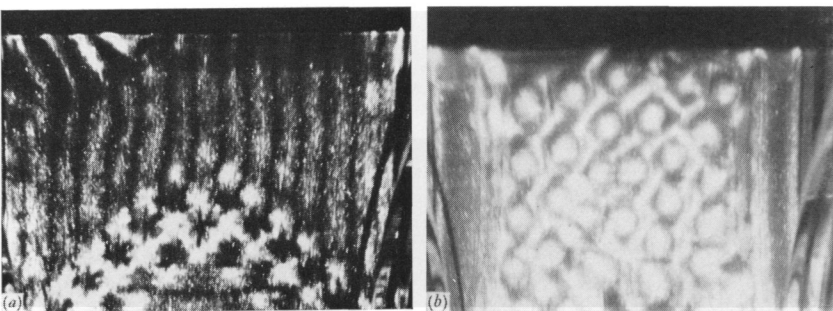


Fig. 7.4. The formation of cells in a square geometry, with solid boundaries above and below. In (a) the mean temperature is fixed, and roll cells form, in (b) it is changing slowly, and hexagons are observed. (From Krishnamurti 1968.)

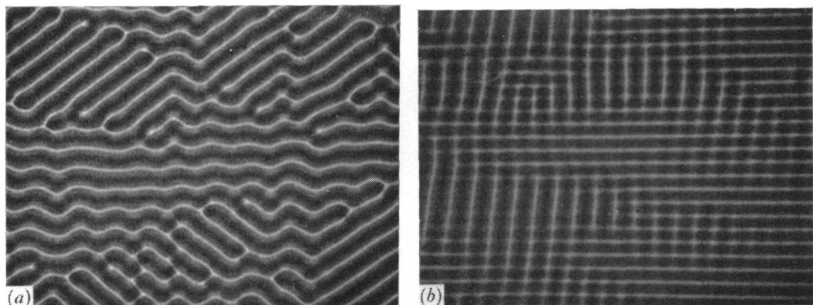


Fig. 7.5. Instability of convection rolls formed on a fluid layer held between two glass plates (a) the zig-zag form, (b) a cross-roll instability. (From Busse and Whitehead 1971.)

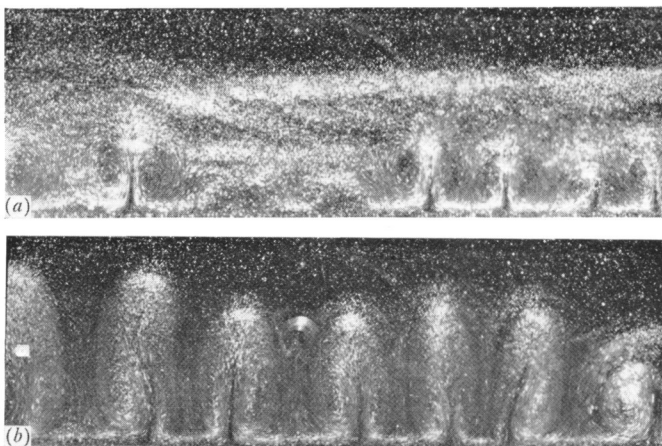


Fig. 7.13. Two stages in the development of a high Rayleigh number flow in silicone oil, marked with aluminium particles, following a sudden increase in temperature of the lower boundary. (From Elder 1968.)

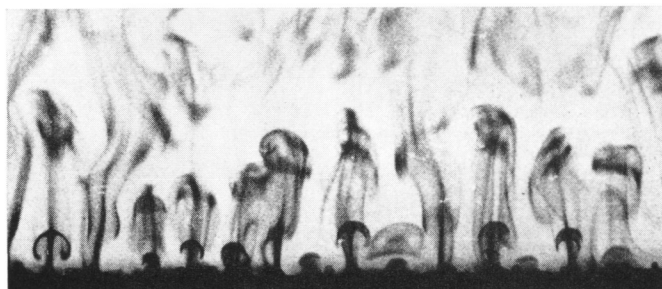


Fig. 7.14. ‘Thermals’ rising from a heated horizontal boundary under a layer of water. (From Sparrow, Husar and Goldstein 1970.)

PLATE XVIII

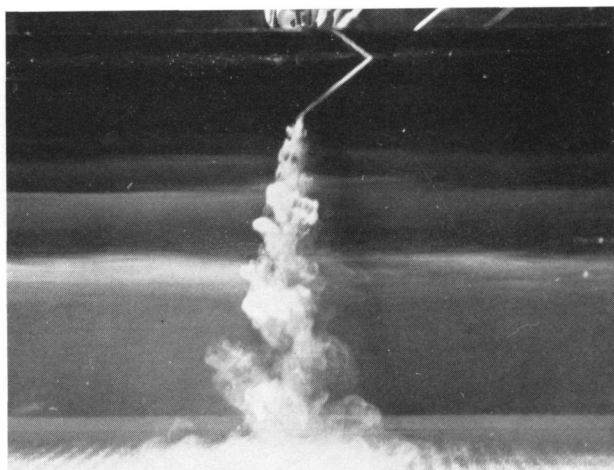


Fig. 7.15. The establishment of a stable stratification by a continuous plume of salt solution in a tank filled initially with fresh water. The layers were formed by the injection of dye at fixed time intervals; more dye was being added when this photograph was taken. (From Baines and Turner 1969.)

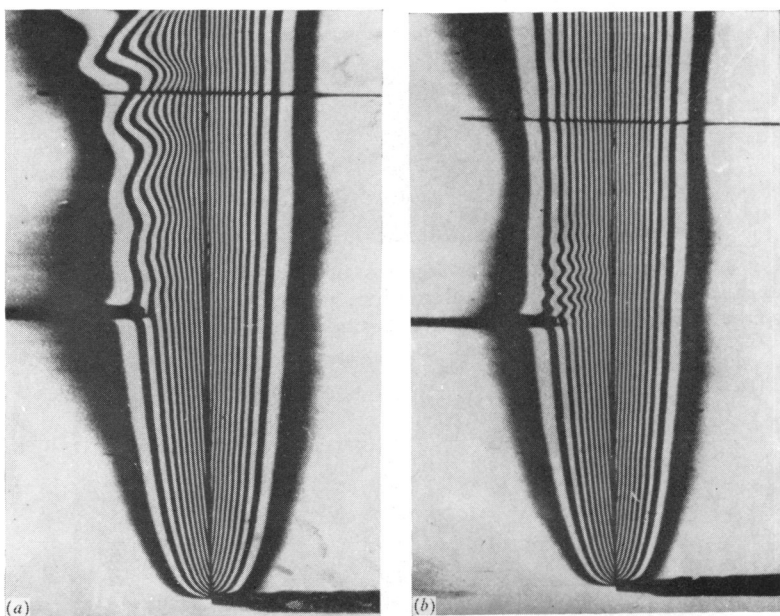


Fig. 7.19. Interferograms of oscillations in the boundary layer near a heated vertical plate. In (a) the disturbance is amplified and in (b) it is damped. (From Polymeropoulos and Gebhart 1967.)

PLATE XIX

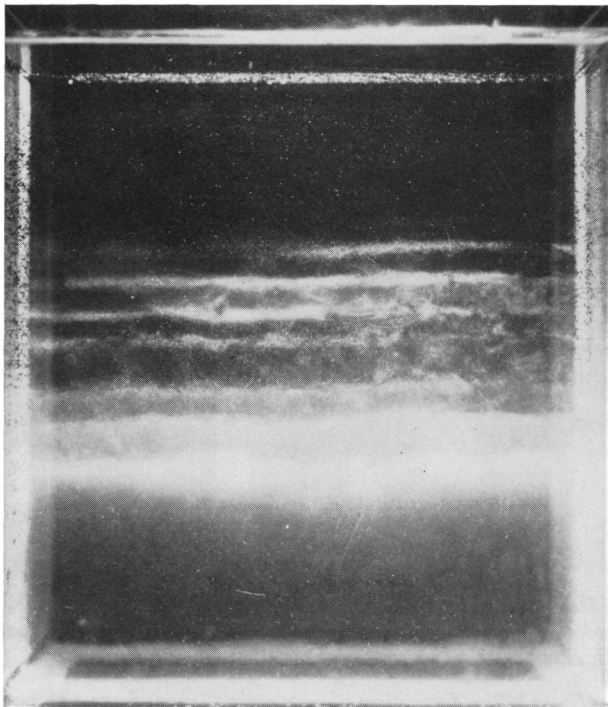


Fig. 8.5. Showing the layers formed in a laboratory tank of smoothly stratified salt solution, by heating from below. The fluid is marked with fluorescein dye (originally put into the bottom layer) and by suspended aluminium powder.

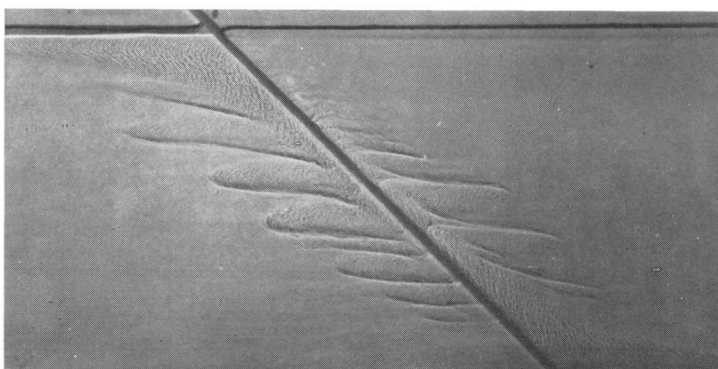


Fig. 8.11. The formation of layers in a two-component system due to the introduction of a sloping boundary. The original distribution of solutes, (linear gradients of NaCl with maximum concentration at the top and zero at the bottom, and of sugar with maximum at the bottom and zero at the top) was stable when contained by vertical walls.

PLATE XX

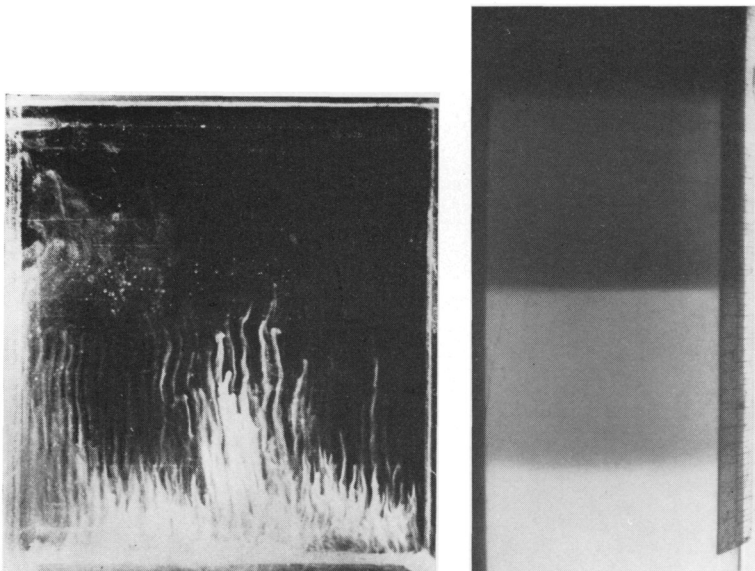


Fig. 8.8. (Left.) Vertical cross-section of salt fingers, marked by fluorescein dye added to the upward moving fingers, and lit with a thin sheet of light perpendicular to the viewing direction.

Fig. 8.9. (Right.) The formation of convecting layers from a smooth stable gradient of salt, driven by a flux of sugar originating in the dark dyed layer at the top. (From Stern and Turner, *Deep-Sea Res.* **16**, 497–511. © Pergamon Press Ltd, 1969.)

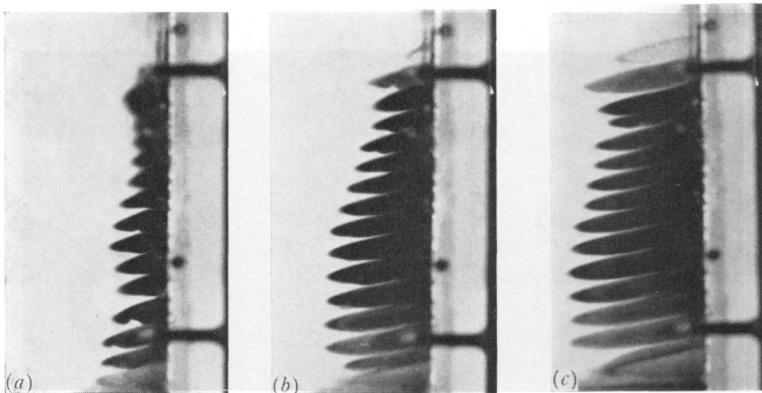


Fig. 8.10. The development of layers in a stratified salt solution subject to heating through a vertical side wall. The photographs were taken (a) 19.5 min, (b) 24 min and (c) 28.25 min after heating began. (From Thorpe, Hutt and Soulsby 1969.)

PLATE XXI

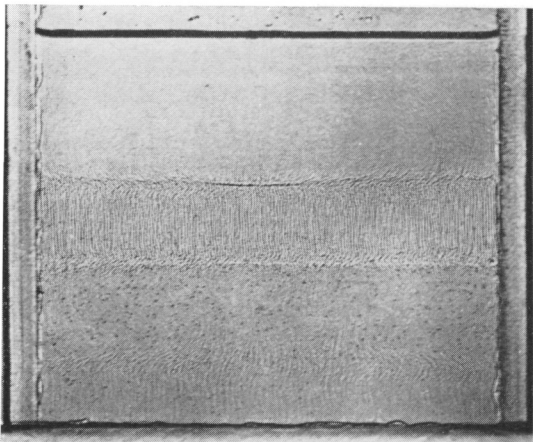


Fig. 8.17. Shadowgraph picture of an interface about $2\frac{1}{2}$ cm deep containing sugar-salt fingers, with convecting layers above and below. (From Shirtcliffe and Turner 1970.)

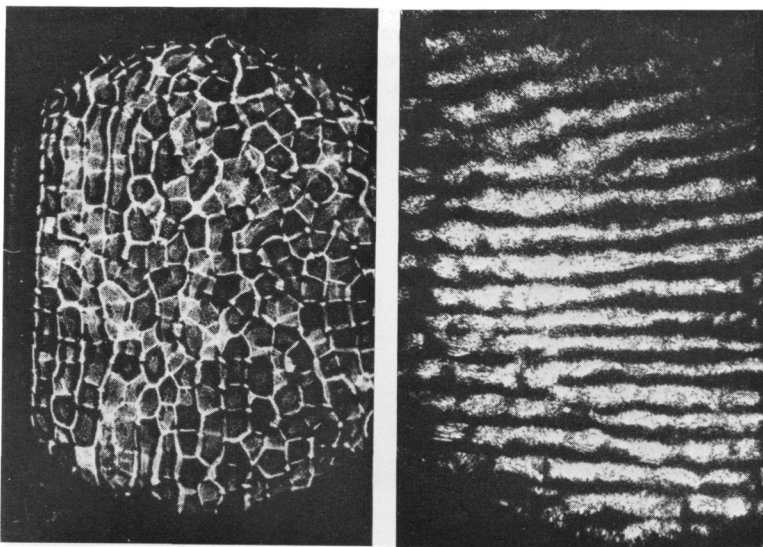


Fig. 8.18. (Left.) Plan view of sugar-salt fingers, obtained by a shadowgraph method. The fingers tend to be square, but with gradually changing orientation, except where they are aligned by boundaries (as at left of picture). (From Shirtcliffe and Turner 1970.)

Fig. 8.19. (Right.) Plan view of a sugar-salt 'finger' interface, across which there is a shear. The fingers are changed into sheets aligned in the direction of the shear. (Photograph: P. F. Linden.)

PLATE XXII

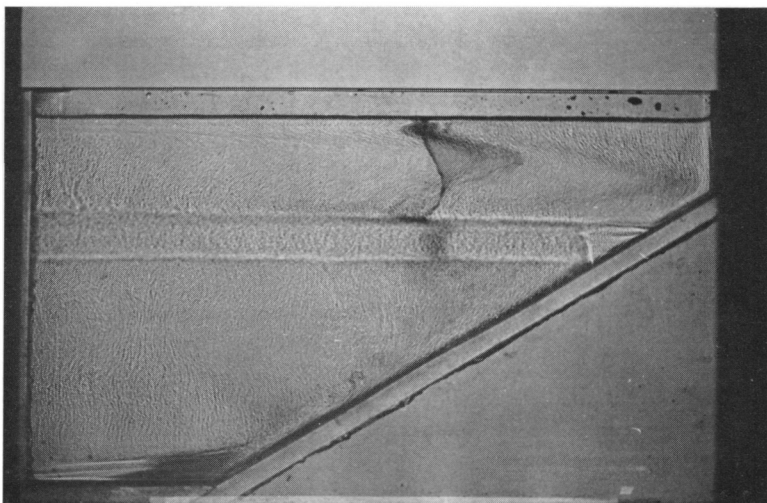


Fig. 8.21. Shadowgraph picture of a two-layer experiment (sugar above salt solutions) in a container with a sloping boundary. The motions are indicated by the distortion of a dye streak. Note the flow right to the bottom, which has produced a reversal of the relative gradients, as indicated by the absence of fingers.

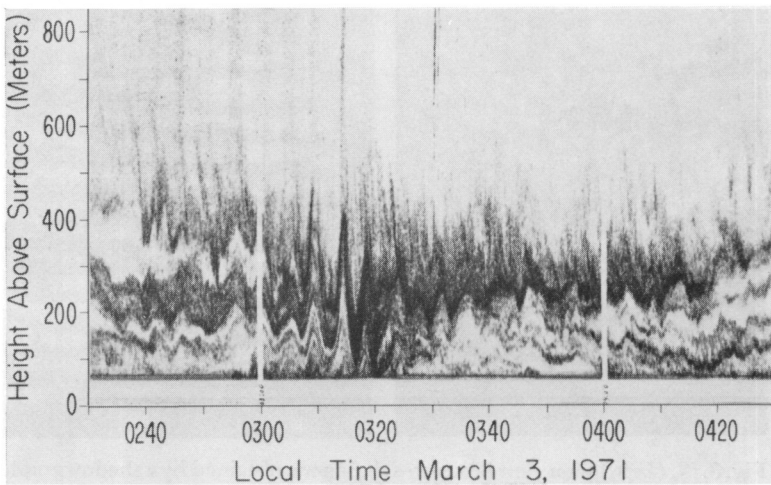


Fig. 10.8. An example of the multiple atmospheric layers observed during the night time radiation inversion, using an acoustic sounding technique. There are many discrete layers, with a widely varying intensity of temperature fluctuations and hence echo strength, all oscillating vertically in phase. (Record obtained by the Wave Propagation Laboratory, NOAA, U.S.A.)

PLATE XXIII

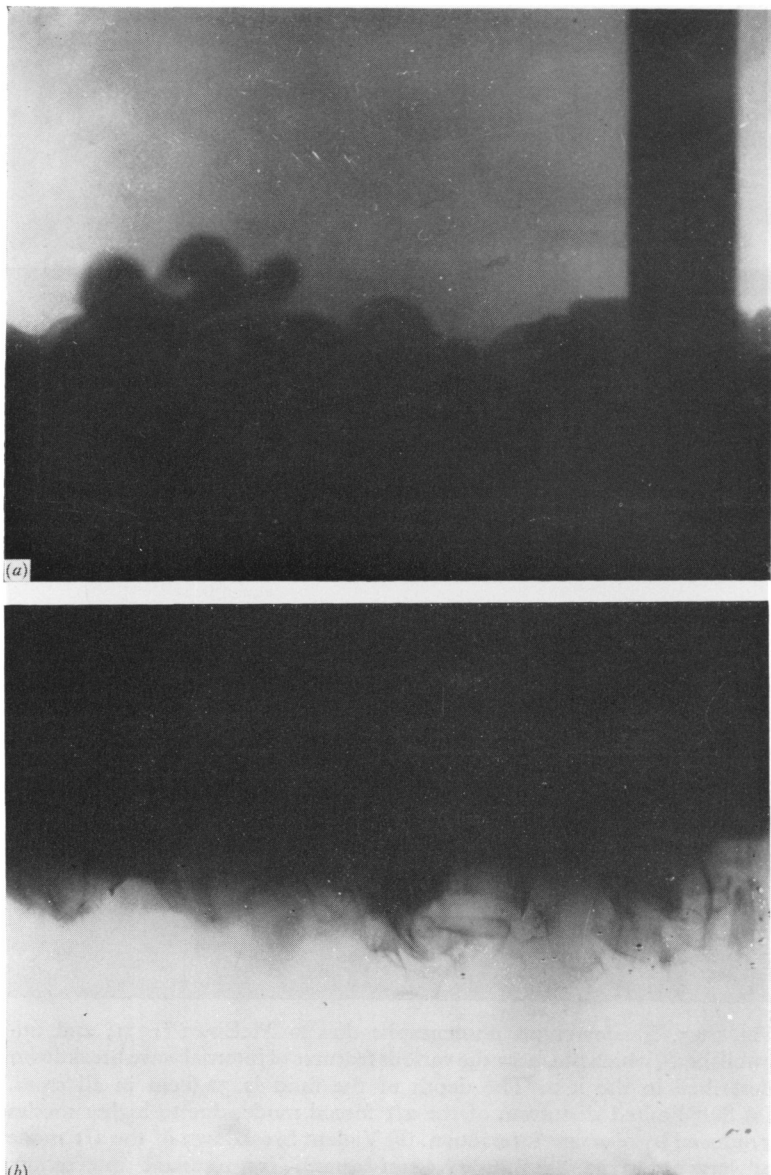


Fig. 9.2. Photographs of a stable interface between salt and fresh water, with stirring on one side of the interface. Dye has been added to (a) the stirred (lower) layer, and (b) the stationary layer. (From Turner 1968*b*.)

PLATE XXIV

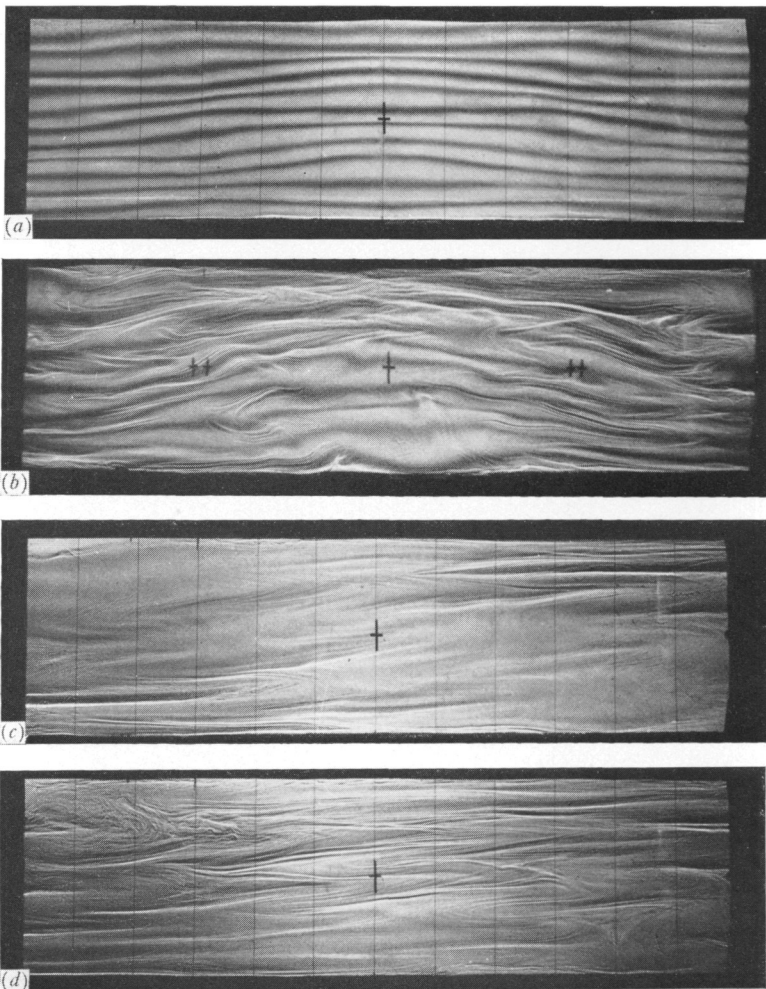


Fig. 10.5. Shadowgraph photographs due to McEwan (1971, and unpublished), which illustrate the various features of internal wave breakdown described in the text. The depth of the fluid is 32.6 cm in all cases. (a) Self-limited distortion of the $2/1$ forced mode, due to higher modes produced by resonant interaction. (b) Violent breakdown of the $2/1$ mode at larger forcing amplitude, again caused by resonant interaction. (c) The growth of instabilities with strong forcing of the $1/1$ mode, a case for which there is no resonant interaction. (d) The same, taken six cycles after (c).